Mon. Not. R. Astron. Soc. **000**, 000–000 (0000) Printed 4 August 2013 (MN LATEX style file v2.2)

Measuring the shock heating rate in the winds of O stars using X-ray line spectra

David H. Cohen,[1⋆] Zequn Li,[1] Kenneth G. Gayley,[2]
Stanley P. Owocki,[3] Jon O. Sundqvist[3,4]
[1] *Swarthmore College, Department of Physics and Astronomy, Swarthmore, Pennsylvania 19081, USA*
[2] *University of Iowa, Department of Physics and Astronomy, Iowa City, Iowa 52242, USA*
[3] *University of Delaware, Bartol Research Institute, Newark, Delaware 19716, USA*
[4] *Institut für Astronomie und Astrophysik der Universität München, Scheinerstr. 1, 81679 München, Germany*

4 August 2013

ABSTRACT

Key words: stars: early-type – stars: winds, outflows – X-rays: stars

1 INTRODUCTION

Embedded wind shocks are the source of the ubiquitous soft X-ray emission seen in O stars. This is confirmed by the significantly Doppler-broadened X-ray emission lines observed with *Chandra* and *XMM-Newton*. The Embedded Wind Shocks (EWS) are generally thought to be associated with the Line Deshadowing Instability (LDI) that is intrinsic to any radiation-driven flow in which spectral lines mediate the transfer of momentum from the radiation field to the matter. Indeed, hydrodynamics simulations show numerous shocks and associated clumped wind structure. However, the level of detail at which the line transport must be modeled is computationally expensive and so simulations have been limited mostly to one dimension, with some 2-D simulations performed but without radiative cooling. Furthermore, resolving shock fronts and the X-ray emitting gas in an advecting wind is extremely challenging, at least partly due to cooling instabilities intrinsic to radiative shocks.

There is currently renewed effort to simulate structured line-driven winds to explore clumping and eventually, X-ray production (Sundqvist & Owocki 2013). There are many open questions that can be addressed from the theoretical side, including whether the bulk of the O star X-ray emission arises from reverse shocks caused by the LDI or from clump-clump collisions involving clumps that arise from the LDI. A related set of questions involves the role played by perturbations at the wind base that can seed the instability. Other, more narrowly focused and quantitative questions include, how efficient is the LDI at producing X-ray emitting plasma? And, what is the distribution of shock strengths produced by the LDI? All these questions await answers from a new generation of 2-D and eventually 3-D models.

⋆ E-mail: cohen@astro.swarthmore.edu

In principle, the observed X-ray emission should provide direct information about the shock heating and thereby constrain future theoretical models and numerical simulations. However, the observed X-ray emission levels from embedded wind shocks in O stars are affected both by the shock heating and by the cooling of the post-shock plasma, which can be through both radiative and non-radiative channels. While the cooling of this post-shock gas involves interesting physics, and while the radiative cooling is the source of the observed X-rays, from the perspective of trying to understand the X-ray production mechanism and constrain physical models, it is the shock heating efficiency and shock strength distribution that we would like to know.

The X-ray emitting wind plasma is usually assumed to be well described by the coronal approximation: statistical equilibrium, with collisional ionization from the ground state balanced by radiative and dielectronic recombination, and collisional excitation from the ground state balanced by spontaneous emission. This gives rise to a spectrum dominated by emission lines from modestly excited states to the ground state, with a small contribution from bremsstrahlung and recombination continuum emission. Each emission line has an emissivity that is a relatively peaked, strong function of temperature, following the temperature dependence of the ionization balance and excitation rates. In this way, each line probes a range of plasma temperatures.

The instantaneous X-ray luminosity from a coronal plasma is simply equal to the combined emissivity of all the lines (and continuum processes) multiplied by the emission measure, which is the volume integral of the density squared. This particular dependence arises from the two-body nature of the excitation process of the emission lines (and of the bremsstrahlung and recombination, for that matter). The temperature distribution of the plasma has thus been traditionally characterized by a differential emission measure

(DEM), $\frac{dEM}{dT}$, which can be described by a continuous function or by a sum of isothermal components, perhaps taken to approximate a continuous distribution with some structure. While subject to various data and analysis constraints and ambiguities, techniques exist for determining a "best-fit" DEM from an observed spectrum. As already pointed out above, though, such a plasma temperature distribution combines both the desired information about shock heating rates and distributions with extraneous and often complex and incomplete information about the cooling history of the hot plasma.

The emission measure is conceptually distant from the shock heating rate for another, related, reason, as well. Namely, the density squared dependence means that a given mass of heated plasma will radiate faster if it is confined to a smaller volume at a higher density. Therefore, the differential emission measure in a post-shock volume will depend not only on the heating rate, but on the local post-shock density, seemingly causing free parameters of any model that might be fit to data to proliferate. However, a key insight about wind shock X-ray emission that makes the analysis much simpler is that for radiative shocks, the overall X-ray luminosity from an ensemble of wind shocks does not depend on the emission measure behind each shock but rather on the kinetic energy flux across each shock front (Owocki et al. 2013). In the strong shock limit, the kinetic energy added as the wind plasma traverses the shock front is converted to thermal energy. And by definition, if the shock is radiative, that thermal energy will be converted to photons.

A related insight we exploit in this paper is that the total energy emitted in any given X-ray emission line as a parcel of wind plasma is impulsively heated, as it passes through a shock and then radiatively cools as it flows downstream from the shock front, is independent of how rapidly the plasma cools. It is, in fact, simply given by the heat injected into the plasma by its passage across the shock front multiplied by the ratio of the emissivity of the spectral line in question to the total emissivity of all the radiative cooling channels, in other words, by the *fraction* of the radiated energy that emerges in the measured line. The luminosity of a given line is thus directly proportional to the rate at which thermal energy is injected into the post-shock wind flow, and thus to the mass-flux across shocks in the wind, and to the square of the shock velocity.

To co-authors: Do we need to make any explicit arguments about steady-state wind conditions to justify associating a snapshot of line luminosities with the complete cooling history of a shock, when only some of the shocks emitting the observed photons have in fact completed their cooling? Or is this implicit assumption obvious, and not in need of any elaboration?

Furthermore, since plasma impulsively heated to a given temperature as it crosses a shock front will radiate at that temperature and, as time goes on, at every lower temperature until it cools back down, an emission line that forms at a given temperature will probe shocks of every higher temperature. And the contribution of a plasma mass parcel to that line will not depend on the heating and cooling history of the parcel, aside from the requirement that the parcel was heated to at least the characteristic temperature of the line. In this way, we can use an ensemble of X-ray emission lines, each with a different temperature dependent emissivity, to derive not only an overall shock heating rate but also to derive the distribution of shock temperatures.

In this paper we apply this analysis to *Chandra* grating spectra of six OB stars with radiative wind shocks driving their EWS X-ray emission (Cohen et al. 2013). The X-ray line profile fitting already performed on these stars enables us to easily apply a wind attenuation correction, which is an important effect for some of the sample stars. This process is much more difficult and introduces degeneracies and ambiguities into the data analysis when carried out in the usual, emission measure-based, global spectral modeling framework. With quantitative information about the shock heating rates in O star winds, we can discuss the derived results in the context of new numerical simulations of LDI-induced wind structure.

To co-authors: We could eliminate the previous paragraph, except for the first sentence, which could become the first sentence of the following paragraph.

In §2 we describe how the measured line fluxes are related to the wind shock heating rate. In §3 we present the results for the program stars. In §4 we discuss the implications of our results in the context of LDI simulations, and we summarize our conclusions in §5.

To co-authors: There are several additional topics that could be added to the intro, including the history of attempts to model the post-shock cooling spectrum (Igor's paper, Zhekov and Palla, etc.); the history of DEM or EM measurements (e.g. Wojdowski and Schulz); the history of LDI simulations. Not sure if we should add any more. Many of these topics will arise in the discussion section, and the context of prior work can be described and acknowledged there.

2 THEORY AND DATA ANALYSIS

For radiative shocks, all the thermal energy injected into the flow as it crosses a shock front eventually appears as radiated photons as the plasma cools from its initial high temperature back down to the ambient wind temperature. While the plasma remains hotter than about 10^6 K, the vast majority of those photons will be X-rays, while at lower temperatures, most of the radiation will be in the EUV, FUV, and UV, and will therefore not be observable by *Chandra* or other X-ray telescopes. For coronal plasmas – low-density, but collisional, plasmas with emission line dominated spectra in which spontaneous emission following collisional excitation from the ground state is the principal emission mechanism – the emission line strengths are characterized by a temperature-dependent emissivity, $\Lambda(T)$, which is not a function of density for most lines. The form of the temperature dependence arises from the dependence of the ionization balance on temperature and, to a lesser extent, from the excitation rate's temperature dependence. In Fig. 1 we show the emissivities of the 16 lines and line complexes we

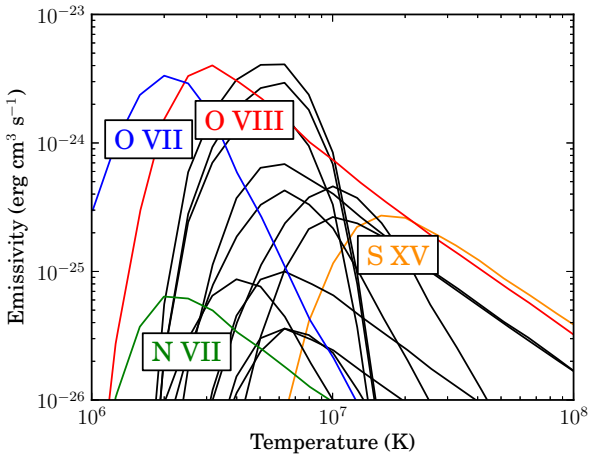

Figure 1. The line emissivity curves from ATOMDB, including all the lines measured in the program stars. The four lines from each of the helium-like complexes are combined together into a single emissivity for each complex. Several important lines at the extremes of the temperature distribution are labeled.

analyze in the O star *Chandra* grating spectra discussed in this paper.

There are many additional weaker lines that contribute to *Chandra* spectra along with continuum processes – bremsstrahlung and recombination – which are relatively weak below 10 to 20 million K. In Fig. 2 we show the total line-plus-continuum emissivity for a coronal plasma, according to ATOMDB (Foster et al. 2012), which is the same source we use for the individual line emissivities. We note that the ATOMDB models assume solar abundances (Anders & Grevesse 1989). More recent re-evaluations of the solar abundance (e.g. Asplund et al. (2009)), as well as abundance variations among the specific program stars, would lead to factors of order tens of per cent adjustments to the line emissivities. We do not account for possible differences in assumed solar abundances or specific star's particular abundances except in a few cases, where non-solar O and N abundances are quite significant. In those cases, we simply scale the ATOMDB emissivities for the relevant lines. We note additionally that traditionally in X-ray astronomy the quantity called *emissivity* has units of ergs cm^3 s^{-1} (and so differs from the traditional per unit volume or per unit mass formulation in standard radiation transfer treatments). With these emissivities in hand, we can compute the fraction of the total radiated power that emerges from the plasma in a given line, at a given temperature, which is demonstrated, graphically, in the right-hand panel of Fig. 2 for the oxygen Lyα line.

The ratio of a given line's emissivity to the total radiated power can be thought of as a branching ratio for that line with respect to all radiative cooling channels. Of course, there can be non-radiative cooling channels as well, including adiabatic cooling and mixing of hot gas with cold gas. The former process will be important in low density winds, while the latter process is more complicated and can occur over a range of conditions, although one situation in which mixing may be likelier to occur is when shock cooling lengths are short and the post-shock region is subject to thin-shell instabilities (Owocki et al. 2013). In this paper we analyze data from massive stars with dense winds, where the shocks are expected to be strongly radiative, and so we ignore adiabatic cooling and assume that almost all of the thermal energy in the shocked wind plasma is converted to radiation as the post-shock gas cools. We justify the neglect of adiabatic cooling for our program stars later in this section and discuss the effects of mixing in §4.

In this picture, then, we should be able to take the measured X-ray line luminosity, and using the line radiation branching ratio described above, compute the rate at which wind plasma is heated to the temperature a given emission line probes, as characterized by its emissivity, shown in Figs 1. Of course, that branching ratio will be temperature-dependent. But as hot gas radiatively cools, it passes through all the temperatures below the initial shock temperature, and so over the lifetime of a parcel of material passing through a shock front and then the post-shock cooling zone, the branching ratio is given by

$$P_\ell \equiv \int_0^\infty \frac{\Lambda_\ell(T)}{\Lambda_{tot}(T)} dT, \qquad (1)$$

where P_ℓ denotes this branching ratio of the line, which we will refer to from now on as the fractional power of the line, $\Lambda_\ell(T)$ is the emissivity of the line as a function of temperature (like the blue curve shown in the right hand panel of Fig. 2), and $\Lambda_{tot}(T)$ is the total emissivity of all radiative processes (the black curve shown in the right hand panel of Fig. 2). P_ℓ has units of temperature, and this temperature can be thought of as the width of the light blue box in Fig. 2, at least to the extent that the total emissivity curve is flat near the peak of the line emissivity. Note that formally, the lower limit of the integral in eqn. 1 should be the ambient wind temperature, rather than zero, but this temperature is generally of order the stellar effective temperature or less, which is obviously well below the lower end of the X-ray temperature regime, and so none of the relevant line emissivities will have a significant contribution at such low temperatures anyway. The upper limit of the integral could also be adjusted to be more physically meaningful, perhaps to some maximum wind shock temperature. We return to this issue later.

To co-authors: Should we just cut the last part of the previous paragraph, about the limits of the temperature integral? We can bring up the idea of a high-temperature cut-off later in the paper without mentioning it here.

With this line fractional power in hand, we can relate the luminosity of any line, L_ℓ, to the thermal energy being deposited in the post-shock gas per unit time via

$$L_\ell = \bar{N} p(T) \dot{M} \alpha \frac{3k}{2\mu m_H} P_\ell, \qquad (2)$$

where $\frac{3}{2}kP_\ell$ is the energy per particle associated with the line fractional power and μ is the usual mean molecular weight per particle while m_H is the hydrogen mass, so that the quantity $\frac{3k}{2\mu m_H P_\ell}$ is the energy radiated in the line per unit mass of wind. The α parameter describes the fraction

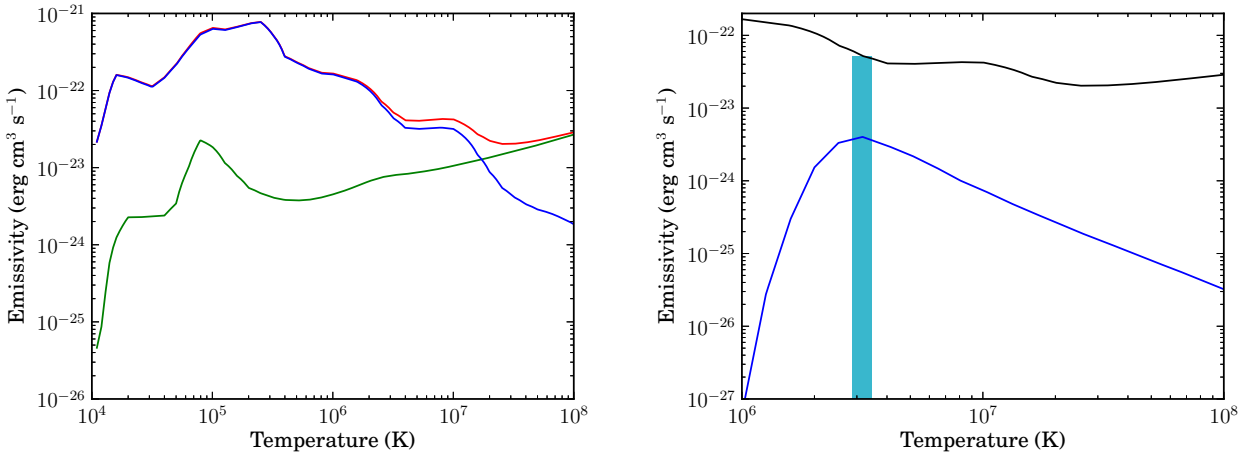

Figure 2. The contribution of all emission lines (blue) to the total radiated power (red), along with the contribution of all continuum processes (green) are shown on the left. On the right is the total power curve (black) with the emissivity of a representative line; in this case, the O VIII Lyα line (blue). The light blue shaded rectangle has the same area as the integrated area under the line emissivity curve. As hot gas cools, we can think of the power radiated in that line as if it were the full thermal content of the plasma but just over the narrow temperature range represented by the horizontal extent of the light blue rectangle.

of the thermal energy that emerges from the plasma as radiation (so $\alpha = 1$ in this study where we assume the cooling is purely radiative, but in principle, with a model for the non-radiative cooling channels, a value of $\alpha < 1$ could be used to parametrize its effects). The stellar wind mass-loss rate is denoted by $\dot{\rm M}$. To relate this to the mass flux through shocks, we simply multiply it by the average number of times a mass parcel traverses a shock front that heats it to a temperature of T or higher. It is useful to express this quantity as the product of $\bar{N}$, the average number of shocks a parcel passes through, and $p(T)$ the probability that a shock achieves a temperature of T or higher. This quantity, $\bar{N}p(T)$, is the key quantity that can be used to constrain models of X-ray production from embedded wind shocks in massive stars, which we can easily calculate, assuming $\alpha = 1$, using

$$\bar{N}p(T) = \frac{2\mu m_H L_\ell}{3\dot{\rm M}kP_\ell}. \quad (3)$$

To reiterate, the product $\bar{N}p(T)$ is a unitless number describing the fraction of wind mass parcels that are shock heated to a temperature of at least T at any point on their flow through the wind.

To co-authors: I was thinking that somewhere around here there could be an explanation of why the emission measure doesn't show up in this analysis at all. But I'm not sure it would be beneficial to our narrative to go down that rabbit hole. And there's that paragraph in §1. Thoughts?

The X-ray spectral data we use to make this measurement are the line fluxes, measured with high-resolution X-ray telescopes – in this study we use data from the *Chandra* High Energy Transmission Grating Spectrometer (HETGS). The line fluxes and wind optical depths for two of the stars in our study, the O supergiants ζ Pup and HD 93129, are available in the literature (Cohen et al. 2010, 2011), while the line fluxes from the other four massive stars in this study were obtained through the same line profile fitting method used in those papers with results described in Cohen et al. (2013). To convert the measured line fluxes into luminosities we apply corrections for (1) the inverse square law via the measured distances to the program stars, (2) the transmission of the interstellar medium, and (3) the transmission of the stellar winds themselves.

The bulk, unshocked component of massive star winds is a source of continuum bound-free opacity to the X-rays emitted by the small fraction of the wind that is shocked. Not only does this opacity lead to attenuation of the X-rays – which we would like to correct for – but it also leads to a characteristic asymmetry of the X-ray line profiles (Owocki & Cohen 2001). The line-profile fitting of the observed X-ray emission lines that we use to find the line fluxes also provides information about the wind optical depth at the wavelength of each line (via the characteristic wind optical depth parameter, $\tau_* \equiv \frac{\kappa \dot{\rm M}}{4\pi R_* v_\infty}$, where κ is the bound-free opacity at the wavelength of the emission line, $\dot{\rm M}$ is the wind mass-loss rate, R_* is the stellar radius, and v_∞ is the stellar wind terminal velocity). From the fitted τ_* values, we can compute the transmission (defined as the fraction of the emitted X-ray radiation that escapes the wind, using the formalism of Leutenegger et al. (2010)). We note that this transmission value is not the usual exponential form due to a slab of absorbing material between the observer and the source, but is a more complicated function that accounts for the spatial distribution of the emitting plasma embedded within the absorbing wind. This wind transmission correction can be significant. In Fig. 3 we show the transmission values for each of the 16 lines measured in the *Chandra* spectrum of ζ Pup, which is the star in our sample with the most wind attenuation.

Given these considerations, the line luminosity, L_ℓ is computed from the observed line flux, F_ℓ from

Table 1. Stellar and Wind Properties

Star	Spectral Type	d (pc)	R_* ($R_\odot$)	v_∞ (km s^{-1})	$\dot{M}$ ($M_\odot$ yr^{-1})	R_a (R_*)	N_{ISM} (10^{22} cm^{-2})
HD 93129A	O2 If*	2300[h]	22.5[a]	3200[a]	$6.8^{+2.8}_{-2.4} \times 10^{-6}$	236	0.41[f]
9 Sgr	O4 V	1780[j]	12.4[b]	3100[e]	$3.7^{+1.0}_{-0.9} \times 10^{-7}$	24	0.22[g]
ζ Pup	O4 If	460[i]	18.9[c]	2250[e]	$1.76^{+0.13}_{-0.12} \times 10^{-6}$	103	0.01[g]
ξ Per	O7.5 III	382[k]	14.0[a]	2450[e]	$2.2^{+0.6}_{-0.5} \times 10^{-7}$	16	0.11[g]
ζ Ori	O9.7 Ib	226[k]	22.1[b]	1850[e]	$3.4^{+0.6}_{-0.6} \times 10^{-7}$	21	0.03[g]
ϵ Ori	B0 Ia	363[d]	32.9[d]	1600[e]	$6.5^{+1.1}_{-1.5} \times 10^{-7}$	31	0.03[g]

References: [a]Repolust et al. (2004); [b]Martins et al. (2005); [c]Najarro et al. (2011); [d]Searle et al. (2008); [e]Haser (1995); [f]Cohen et al. (2011); [g]Fruscione et al. (1994); [h]Townsley et al. (2011); [i]Markova et al. (2004); [j]Sung et al. (2000); [k]van Leeuwen (2007); all mass-loss rates from Cohen et al. (2013)

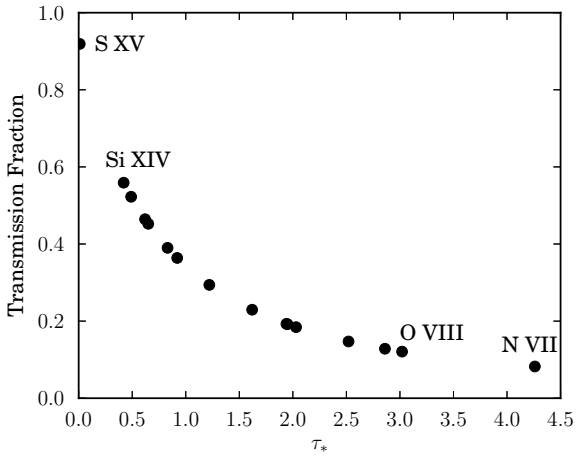

Figure 3. The fraction of the emitted line photons that are transmitted through the wind without being absorbed, for each line in the *Chandra* spectrum of ζ Pup, as a function of each line's characteristic optical depth value, τ_*, derived from fitting the line profile shapes.

$$L_\ell = 4\pi d^2 F_\ell e^{\tau_{ISM}} / T_w(\tau_*), \quad (4)$$

where d is the distance to the star, τ_{ISM} is the optical depth of the interstellar medium, which we compute from the observed ISM column densities and the TBABS ISM absorption model (Wilms et al. 2000), and $T_w(\tau_*)$ is the wind transmission (which is denoted as $T(\tau_*)$ in Leutenegger et al. (2010) but which we slightly relabel here to make it distinct from the temperature).

For each of the stars we analyze, we list in Table 1 the relevant stellar and wind parameters. We include the adiabatic radius, R_a, which is the radius at which the radiative cooling length of a typical shock is equivalent to the stellar radius (Owocki et al. 2013). Below that radius, shocks cool primarily by radiation, while above it, adiabatic expansion dominates the cooling. The vast majority of X-ray emission from embedded wind shocks in massive stars comes from the first several stellar radii of the wind, and thus the values of R_a listed in the table justify our assumption of radiatively cooled shocks in the program stars.

Table 2. Power Law Fits to $\bar{N}p(T)$ Values

Star	Spectral Type	N_o	α
HD 93129A	O2 If*	62	-3.55
9 Sgr	O4 V	0.34	-2.08
ζ Pup	O4 If	0.64	-2.18
ξ Per	O7.5 III	0.27	-2.17
ζ Ori	O9.7 Ib	0.23	-2.19
ϵ Ori	B0 Ia	0.30	-2.59

3 RESULTS

The shock heating rates computed using eqn. 3 for each emission line in each of the program stars are plotted in Fig. 4 as a function of the lines' temperatures of peak emissivity. For each star, different lines that probe similar temperature ranges give consistent results. And there is clearly a decreasing trend for each star, consistent with the cumulative, monotonic nature of the probability function, $p(T)$. We note, also, that applying the wind and ISM transmission corrections improved the consistency of the results, as did accounting for lower oxygen and higher nitrogen abundances in ζ Pup (Bouret et al. 2012) and several other stars.

Uncertainties on the derived $\bar{N}p(T)$ values come from several different sources. The biggest are the uncertainties on the wind mass-loss rates, although that error will affect every line from a given star the same amount and so will simply scale the overall shock heating rate for a given star up or down. Other sources of error derive from uncertainty in the distances, the X-ray profile fitting derived optical depths, τ_*, and the associated wind transmission correction, the ISM transmission, and statistical errors on the line flux measurements. Taking all these into account, we represent the combined uncertainties by the vertical extent of the gray boxes in Fig.4.

We fit a power law to each star's shock heating rate – the ensemble of $\bar{N}p(T)$ values – which we show in each panel of Fig.4 and all together in Fig. 5. The power law has the simple form

$$\bar{N}p(T) = N_o \left(\frac{T}{10^6 \mathrm{K}}\right)^\alpha. \quad (5)$$

We list the best-fit power law model parameters, N_o and α, in Table 2.

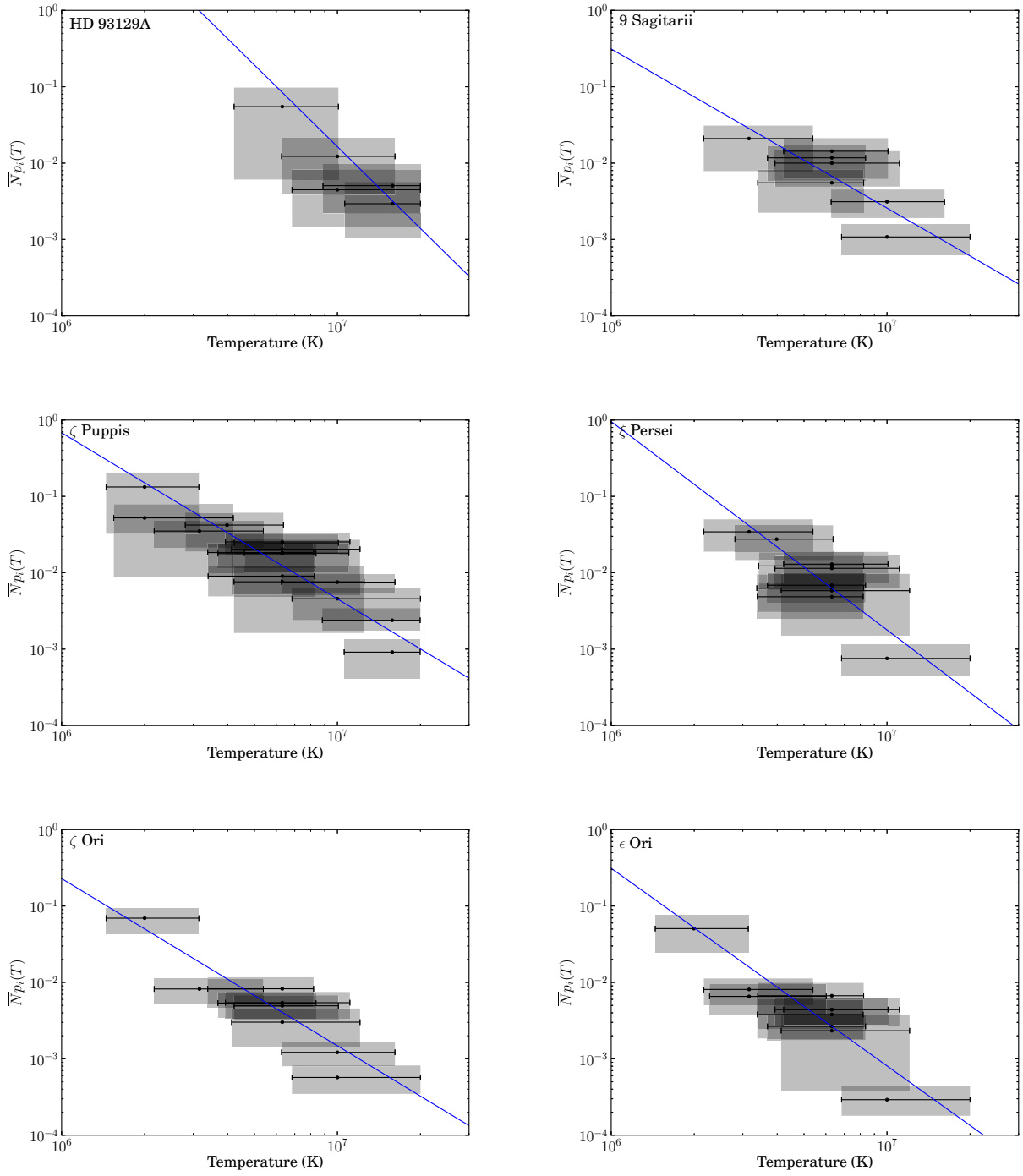

Figure 4. The shock heating rate, $\bar{N}p(T)$, is shown with the uncertainty on its value as well as the FWHM of the line emissivities denoted by the extent of the gray rectangles. The best-fit power law to each set of values is shown as a blue line in each panel.

4 DISCUSSION

Co-authors: This section is much more provisional than the first three. In fact, only the first three paragraphs are actual draft text; all the subsequent stuff, in italics, are questions about various potential topics of discussion. Suggestions are welcome!

The results for all six stars look quite similar, with the $\bar{N}p(T)$ shock heating rate consistent with a power law of index slightly steeper than $\alpha = -2$ and something approaching or exceeding a majority of the wind mass passing through a shock of $T > 10^6$ K. The earliest star in the sample, HD 93129, is perhaps an exception, with a steeper slope and a higher overall probability, but this star also has the lowest quality data and the fewest lines, and its difference

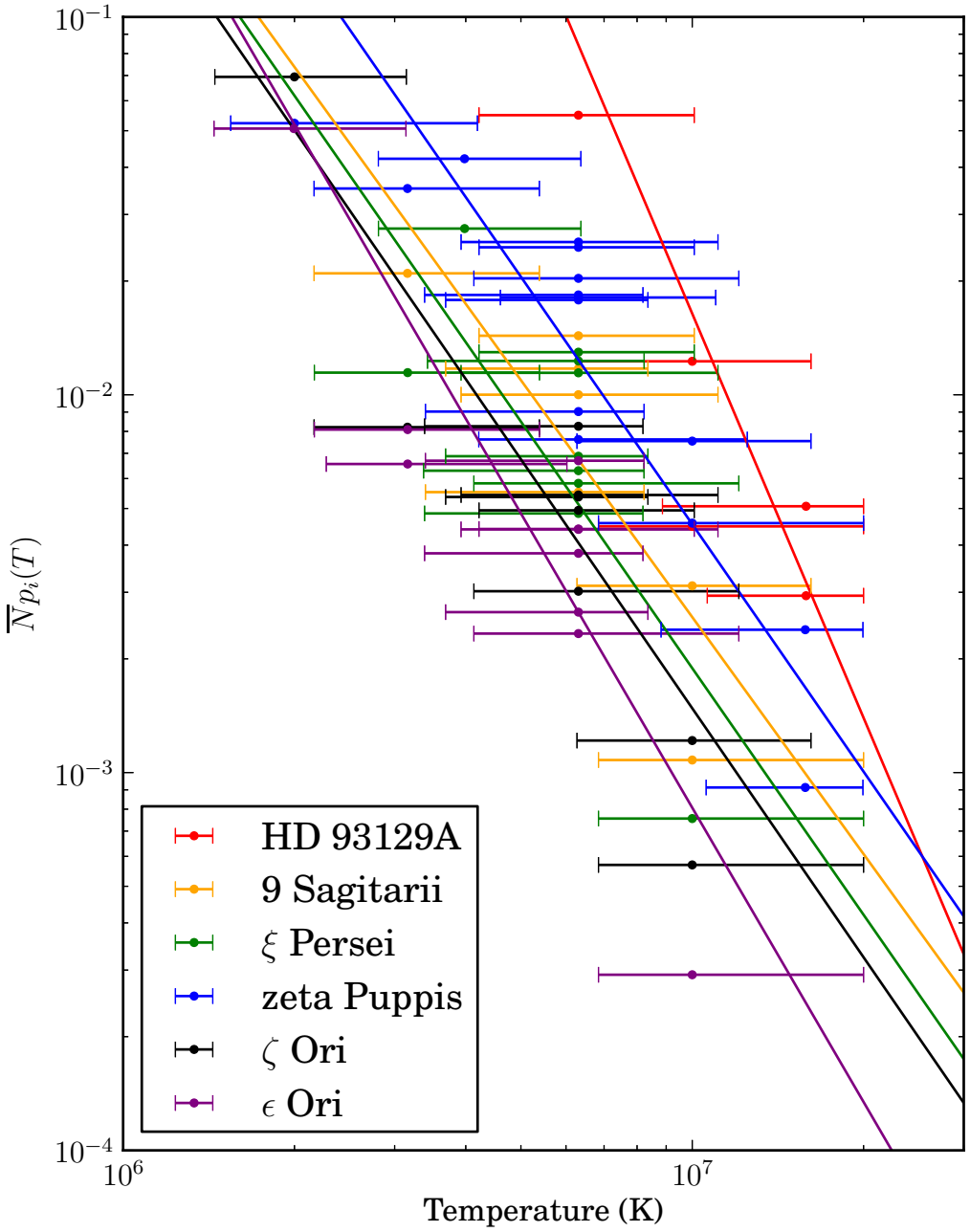

Figure 5. The shock heating rate, $\bar{N}p(T)$, derived from each line of each of our program stars. The horizontal location of each point corresponds to the temperature of peak emissivity of that line, while the horizontal bars represent the FWHM of the emissivity curves. The colored lines are best-fit power law models. These are the same results shown in Fig. 4 but simply collected together to facilitate comparison. We do not show the uncertainties on each point – corresponding to the vertical extent of the gray boxes – to keep the plot from being too cluttered.

from the rest of the sample may not prove to be statistically significant.

The strong negative slope is somewhat mitigated by the fact that $p(T)$ is defined to be the probability of a shock heating a mass parcel to temperature T or higher, and so $p(T)$ is a cumulative distribution. The differential distribution, describing the probability that a shock has a certain temperature, would be a power law with an index lower by one, so with an index $\alpha \approx -1$. This is still a strongly decreasing function, implying that a shock is more than ten times as likely to heat the wind to one million K as it is to ten million K. This is a specific, quantitative constraint on numerical simulations of embedded wind shocks, as is the result $N_o \approx 1$, implying that many or most mass parcels in a wind pass through one shock of sufficient strength to heat it to one million K.

We have performed some 1-D radiation hydrodynamics simulations of an O star wind, using the VH-1 code an implementing the smooth source function approximation for the line force. The instability is self excited in these simulations, with no base perturbations of the wind and no limb darkening included. The wind structure generated in these simulations is similar to that seen in Runacres & Owocki (2002), for example. In Fig. 6 we show the output of this simulation in several different ways, focusing on the distribution and frequency of shocks. This simulation shows a steep decline in shock frequency with shock jump velocity, or temperature. Perhaps the decline is even steeper than the $p(T) \approx T^{-2}$ we infer from our data analysis, and also perhaps significantly fewer mass parcels pass through strong shocks overall. *For more definitive interpretation, we should probably look at LDI simulations with base perturbations.*

What about the characterization of the temperature sensitivity of each line? Does it make sense to just use the emissivity curve? Or should it be weighted by the fractional line power – in other words, divided by the total emissivity curve? A centroid of that weighted function could be used. Zack has tried this, and it pulls lines with high energy tails in their emissivities pretty far to the right. On the flip-side, it could be argued that the temperature range denoted for each line should be weighted by the derived NpT function itself, since many shocks will heat plasma up to a temperature somewhere within the range of a given line's emissivity and thus it is only the rare shock that samples the high energy tails. Perhaps these two effects basically cancel and so just using the FWHM is fine. Should we even discuss any of this?

How do these results relate to previous DEM determinations (which also show a relatively steep decline of emission measure with temperature)?

What about neglected non-radiative cooling? Neglected cooling channels would imply we've underestimated $\bar{N}p(T)$. Adiabatic cooling will be more important for hotter gas and stronger shocks. So to the extent we've incorrectly neglected adiabatic cooling, we would overestimate the steepness of the power-law fits. Any neglected mixing, while also leading to an underestimate of the shock heating rate, might have the opposite effect on the slope of the heating rate, as radiative shocks might be more likely to suffer non-radiative cooling via mixing, given their susceptibility to thin-shell instabilities.

5 CONCLUSIONS

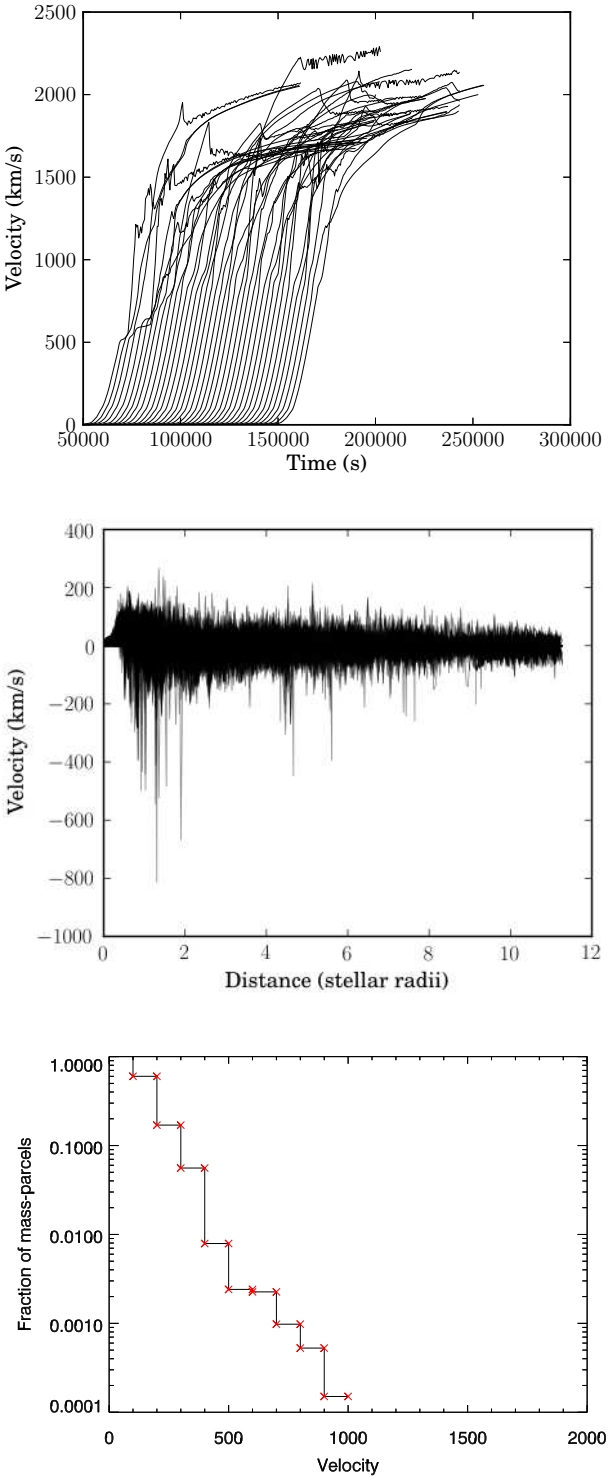

Figure 6. *Co-authors: these figures and caption are preliminary.* The velocity histories of many mass parcels as they advect through the wind in a 1-D hydro simulation with no seeding of the LDI at the wind base; simply self-excited LDI structure (top). The characteristic reverse shocks induced by the LDI can be seen as sudden decelerations, or horizontal segments. Shock jumps for each mass parcel can be calculated and plotted (middle) to show the magnitude and spatial distribution of the wind shocks. And the frequencies of shocks of a given velocity range can be calculated and plotted (bottom). These shock jump velocities are directly proportional to the post-shock temperature.

ACKNOWLEDGMENTS

Support for this work was provided by the National Aeronautics and Space Administration through *Chandra* award numbers...

REFERENCES

Anders E., Grevesse N., 1989, Geo. Cosm. Acta, 53, 197
Asplund M., Grevesse N., Sauval A. J., Scott P., 2009, ARAA, 47, 481
Bouret J. C., Hillier D. J., Lanz T., Fullerton A. W., 2012, A&A, 544, 67
Canizares C. R., et al., 2005, PASP, 117, 1144
Cohen D. H., Gagné M., Leutenegger M. A., MacArthur J. P., Wollman E. E., Sundqvist J. O., Fullerton A. W., Owocki S. P., 2011, MNRAS, 415, 3354
Cohen D. H., Leutenegger M. A., Wollman E. E., Zsargó J., Hillier D. J., Townsend R. H. D., Owocki S. P., 2010, MNRAS, 405, 2391
Cohen D. H., Wollman E. E., Leutenegger M. A., Sundqvist J. O., Fullerton A. W. A., Zsargó J., Owocki S. P., 2013, MNRAS, submitted
Dessart L., Owocki S. P., 2003, A&A, 406, L1
Dessart L., Owocki S. P., 2005, A&A, 437, 657
Feldmeier A., Puls J., Pauldrach A. W. A., 1997, A&A, 322, 878
Foster A. R. Ji L., Smith R. K., Brickhouse N. S., 2012, ApJ, 756, 128
Fruscione A., Hawkins I., Jelinsky P., Wiercigroch A., 1994, ApJS, 94, 127
Haser S. M., 1995, Universitäts-Sternwarte der Ludwig-Maximillian Universität, München
Leutenegger M. A., Cohen D. H., Zsargó J., Martell E. M., MacArthur J. P., Owocki S. P., Gagné M., Hillier D. J., 2010, ApJ, 719, 1767
Markova N., Puls J., Repolust T., Markov H., 2004, A&A, 413, 693
Martins F., Schaerer D., Hillier D. J., 2005, A&A, 436, 1049
Najarro F., Hanson M. M., Puls J., 2011, A&A, 535, 32
Owocki S. P., Castor J. I., Rybicki G. B., 1988, A&A, 335, 914
Owocki S. P., Cohen D. H., 2001, ApJ, 559, 1108
Owocki S. P., Sundqvist J. O., Cohen D. H., Gayley K. G., 2013, ApJ, 429, 3379
Repolust T., Puls J., Herrero A., 2004, A&A, 415, 349
Runacres M. C., Owocki S.P., 2002, A&A, 381, 1015
Searle S. C., Prinja R. K., Massa D., Ryan R., 2008, A&A, 481, 777
Sundqvist J. O., Owocki S. P., 2013, MNRAS, 428, 1837
Sung H., Chun M.-Y., Bessell M. S, 2000, AJ, 120, 333
Townsley L. K., et al., 2011, ApJS, 194, 1
van Leeuwen F., 2007, A&A, 474, 653
Wilms J., Allen A., McCray R., 2000, ApJ, 542, 914